



Enhancing the virtual reality optical efficiency via emission cone optimization of the display panel

ZHENYI LUO, YEFU ZHANG, YUQIANG DING, AND SHIN-TSON WU* 

College of Optics and Photonics, University of Central Florida, Orlando, Florida 32816, USA

**swu@creol.ucf.edu*

Abstract: The pancake lens, also referred to as a polarization-based catadioptric lens, is commonly employed as the imaging lens in virtual reality (VR) headsets due to its compact design and superior image quality. However, the pancake lens significantly reduces the optical efficiency to about 12.5% if the incident light is unpolarized, primarily due to the use of a half-mirror. To boost system efficiency, we analyze how the display panel's emission cone affects optical efficiency. By incorporating brightness enhancement films (BEFs) to tailor the angular distribution of the emitted light, the optical efficiency can be improved by 65.2%.

© 2025 Optica Publishing Group under the terms of the [Optica Open Access Publishing Agreement](#)

1. Introduction

Providing fully immersive experiences, virtual reality (VR) display has the potential to revolutionize the ways we perceive and interact with the digital world [1–5]. To ensure excellent image quality over a large field-of-view (FOV) while remaining a compact formfactor, pancake lens has been widely used in VR systems to magnify the image from the microdisplay panel [6]. Despite these advantages, the pancake lens suffers from a low optical efficiency of just 12.5% for unpolarized input light, which in turn increases the power consumption and thermal effect of the VR headsets [7,8].

Figure 1(a) depicts the VR system configuration with a pancake lens. Light emitted from the microdisplay panel first passes through a circular polarizer (CP), converting it into circularly polarized light. However, due to the presence of a half-mirror (HM) in the pancake lens, one half of this circularly polarized light is reflected and lost. The remaining portion undergoes two reflections, one at the reflective polarizer (RP) and another at the HM, while a quarter-wave plate (QWP) modulates its polarization state. Ultimately, the light passes through the pancake lens and reaches the user's eye. The maximum efficiency of both the CP and the HM is 50%. With three interactions involving these optical components, the overall system efficiency drops to 12.5%. Tremendous efforts have been devoted to addressing this low-efficiency issue by developing more advanced folding structures [9–11]. However, these believed to be novel configurations often have trade-offs, such as increased system volume or reduced performance due to the employed polarization films. Optimizing panel's emissions using liquid crystal optics has also been conducted [12,13]. However, the chromatic aberration of such diffractive components [14–16] limits their further applications. Moreover, these prior studies have primarily focused on the VR systems with refractive lenses, which are bulky and heavy.

During the pancake lens design process shown in Fig. 1(b), the chief ray incident angles for different fields on the display are typically constrained to small values to enhance the overall brightness, as the light intensity is stronger near the optical axis of the display panel. Moreover, a larger emission cone is more likely to generate stray light [17], which can degrade the contrast of the VR system, as depicted in Fig. 1(c). In Fig. 1(c), the blue rays represent the signal light path, while the red and green rays with large exit angles after the microdisplay light source indicate the

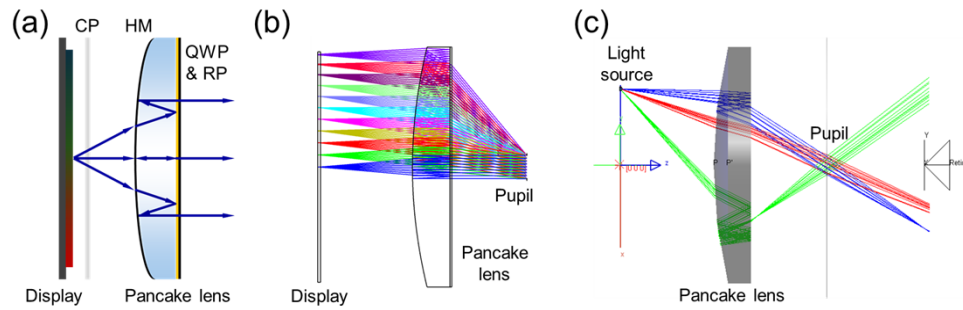


Fig. 1. (a) System configuration of a pancake VR system. (b) Design of a pancake lens. (c) Ray simulation in a pancake VR system. CP: circular polarizer; HM: half mirror; QWP: quarter-wave plate; RP: reflective polarizer.

stray light paths. Therefore, the display emission cone plays a crucial role in determining both the brightness and contrast of the entire VR system.

In this paper, we investigate the impact of the display panel's emission cone on the pancake VR system performance. By optimizing the emission cone design, we are able to boost the optical efficiency by $\sim 65.2\%$.

2. Simulations and results

The emission cone of the display panel is closely related to the exit pupil size of the VR system. To explore this relationship, we first conducted simulations in LightTools to analyze how the display emission cone affects the illuminated area size on the pupil plane. Figure 2(a) illustrates the cross-sectional illumination profiles on the pupil for different emission cones. All the light sources considered here are assumed to exhibit a Lambertian angular distribution. Different emission cones are achieved by constraining their emission angle. The bandwidth for the 0° emission cone is initially zero and gradually increases as the emission cone enlarges. The diameter of the human eye pupil varies between 2 mm and 8 mm under different lighting conditions. The full width at half maximum (FWHM) of the $\pm 10^\circ$ emission cone is approximately 8 mm. Therefore, the minimum emission cone required to produce an exit pupil larger than the diameter of the eye pupil is $\pm 10^\circ$.

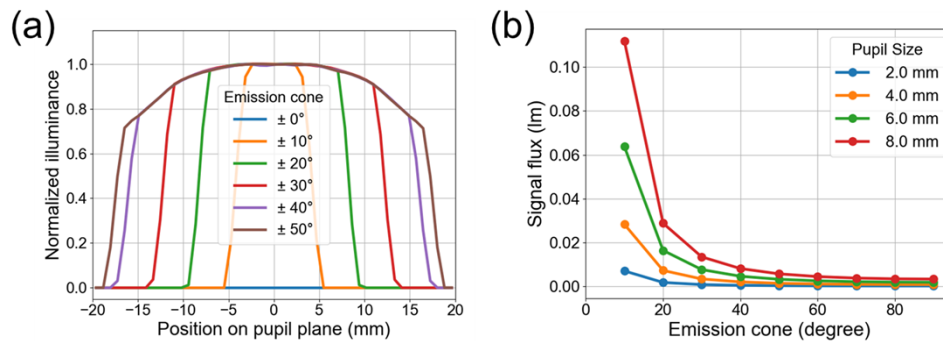


Fig. 2. (a) Cross-sectional illuminance profiles for different emission cones. (b) Impact of emission cones on signal flux.

We also simulated the signal flux received by the eye model and the results are plotted in Fig. 2(b). The photometric flux of the light source, positioned at the center of the panel, is maintained at 1 lumen while varying the emission cone angles. For a constant pupil size, the

received signal flux exhibits a marked reduction as the emission cone increases. Specifically, for a 4-mm pupil size, the received signal illuminance for the $\pm 10^\circ$ emission cone is more than 30x higher than that for the $\pm 90^\circ$ emission cone. This is attributed to the fact that the beam size after the pancake lens is governed by the emission cone of the light source. Given that the eye's pupil size remains fixed, a larger beam size produced by a broader emission cone leads to increased light loss, because a greater portion of the beam falls outside the pupil's aperture. A larger pupil's size helps reduce the light loss, as shown in Fig. 2(b). Theoretically, the maximum signal flux is 0.125 lumen if all the emitted light from the source can be captured by the pupil, as previously introduced.

Next, we conducted simulations to investigate the signal flux and signal-to-noise ratio (SNR) for different emission cone angles, source positions, and pupil sizes. The source positions are directly related to the field angle incident in the user's eye, as shown in Table 1.

Table 1. Source positions vs. Field angles

Source positions (mm)	0	4	8	12	16	20
Field angles (degree)	0	9.5	19.3	29.4	39.9	51.7

Figure 3(a) presents the signal flux heatmap for different pupil sizes. A larger pupil size captures more light, resulting in a higher signal flux. Meanwhile, a smaller emission cone enhances the received light by producing a more concentrated beam. As the source position on the panel moves away from the center, the signal illuminance decreases due to aberrations at larger field angles. The simulated SNR results are illustrated in Fig. 3(b). The observed SNR appears to be independent of pupil size, because both signal and stray light intensities increase proportionally with a larger pupil. However, SNR does depend on the emission cone. A smaller emission cone reduces the potential paths for stray light, as Fig. 1(c) depicts, thereby leading to a higher SNR. Meanwhile, sources positioned farther from the panel center exhibit a higher SNR compared to those at the center, due to different stray light paths.

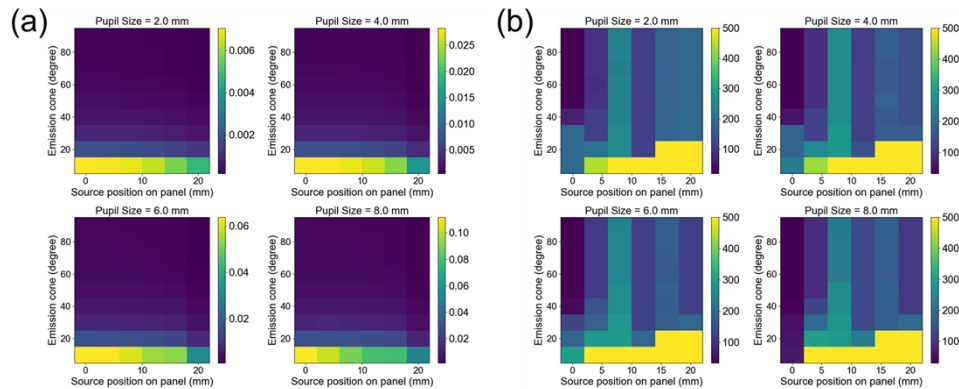


Fig. 3. (a) Signal flux and (b) signal-to-noise ratio (SNR) for varying emission cone angles, source positions, and pupil sizes.

A smaller emission cone appears to enhance signal flux and consequently improve system efficiency, as indicated by our simulations. However, the emission cone modulation process must be considered to narrow the emission cone from a Lambertian source with a $\pm 90^\circ$ emission.

Liquid crystal displays (LCDs) are the dominant microdisplay panels for VR devices on the market, primarily due to their low cost and satisfactory performance [18], especially when compared to micro-OLED displays, which tend to be much more expensive. Tremendous efforts have been made over the past decades to control the angular distribution of the emitted

light from an LCD, a technology commonly referred to as directional backlighting. Brightness enhancement films (BEFs), shown in Fig. 4(a) and 4(b), are optical films for shaping the backlight distribution profiles [19,20]. Each BEF consists of microprism structures that focus the light on the perpendicular direction. Two crossed BEFs are laminated together to shape the emission cone in both longitudinal and latitudinal directions. A reflective film is used to recycle the reflected light, thereby enhancing the overall efficiency. In addition to BEFs, a microlens array (MLA) can control the display's emission cone by redistributing the light output. However, compared to MLAs, BEFs offer several advantages. They can be fabricated using cost-effective extrusion processing [21], making them more suitable for large-scale production. In contrast, MLAs require intricate replication technologies to achieve the necessary precision [22], increasing manufacturing complexity and cost. Additionally, BEFs are generally thinner than MLAs, allowing for easier integration into a compact display module without significantly increasing the overall thickness. Adding a diffuser is another approach to control the angular distribution of an LCD [23,24]. A scattering type of diffuser is typically combined with BEFs in an LCD to generate a wide-angle Lambertian distribution for the light before it enters the BEFs. A refraction-type diffuser may offer more design flexibility, but it comes with a more complicated fabrication process. Given the advantages of low cost and thin-film structure, BEFs are promising candidates for VR applications.

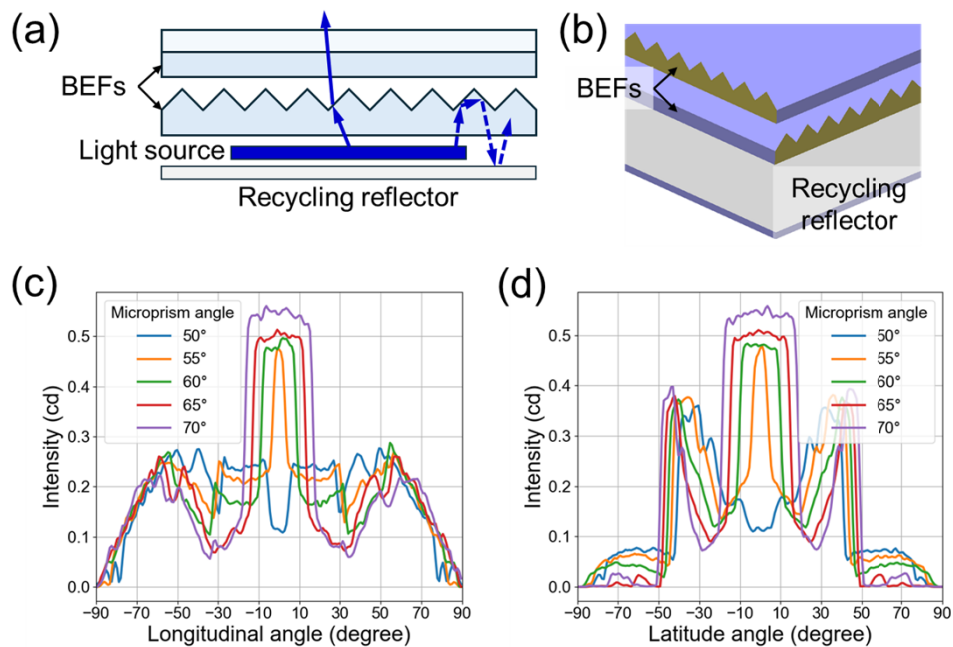


Fig. 4. (a) Crossed BEFs for emission cone modulation. (b) BEF simulation model. Angular distribution modulated by crossed BEFs in (c) longitudinal and (d) latitude directions.

Our simulation results in Fig. 4(c) and 4(d) indicate that BEFs can focus light into a small emission cone, and the emission cone can be modulated by adjusting the microprism angle. However, a microprism angle of 50° somewhat degrades the emission cone modulation function. Given the minimum emission cone of $\pm 10^\circ$ required for the pupil size, we will explore using a microprism angle greater than 60° .

To further investigate the performance of BEFs in modulating the emission cone, we define the bandwidth of the central peak in Fig. 4(c) and 4(d) as the emission cone, representing the angular range where most of the emitted light is concentrated. Figure 5(a) illustrates the variation in the

emission cone as the microprism angle increases. A larger microprism angle results in a wider emission cone. Additionally, we investigate the impact of microprism pitch on the emission cone while keeping the pitch constant when adjusting the microprism angle. Our simulation results indicate that the modulated emission cone is independent of the microprism pitch. Two different materials, PMMA ($n = 1.5$) and NBK7 ($n = 1.52$), exhibit different emission cone modulation when adjusting the microprism angle. A higher refractive index appears to result in a narrower emission cone. Furthermore, the modulation efficiency of BEFs is depicted in Fig. 5(b), where only the light within the emission cone range is considered for the efficiency calculations. The efficiency increases as the microprism angle increases. Additionally, a smaller pitch enhances efficiency slightly, but a higher refractive index leads to slightly decreased efficiency.

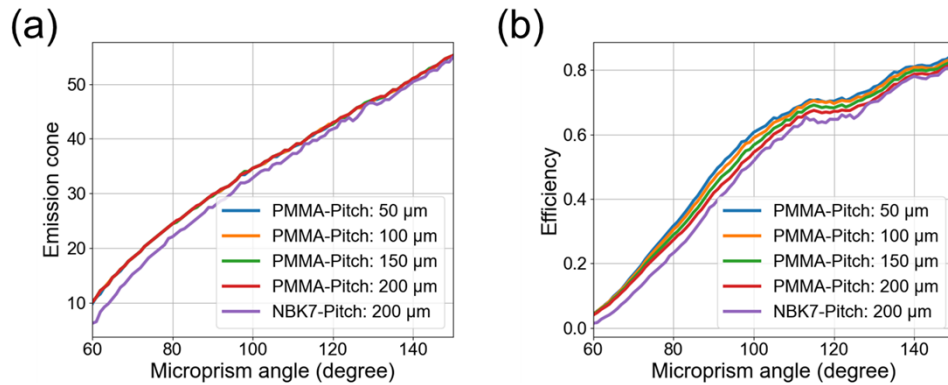


Fig. 5. (a) Emission cone and (b) efficiency variation when adjusting the microprism angles.

Compared to a Lambertian source with $\pm 90^\circ$ emissions, BEFs can achieve higher efficiency within the same emission cone, as Fig. 6(a) shows. The blue line represents the flux received within different emission cone ranges from the Lambertian source, while the red line illustrates the efficiency-emission cone relationship discussed in Fig. 4(c) and 4(d). The efficiency of BEFs can be up to twice that of a Lambertian source for specific emission cones. The diffraction effect of the microprism structure in BEFs has also been evaluated. The total transmission for pitches ranging from $50\ \mu\text{m}$ to $200\ \mu\text{m}$ exceeds 95% within the ± 2 diffraction orders when the microprism angle is set at 90° . The diffraction angle for the $50\text{-}\mu\text{m}$ pitch is 1.26° for the second-order diffraction, and it decreases as the pitch value increases. Therefore, the impact of the diffraction effect can be neglected in our system simulations.

After individually evaluating the performance of the BEFs, we also integrated the BEF structure with the pancake VR system to assess the overall improvement. Figure 6(b) illustrates the flux received by the pupil for different source positions as the microprism angle increases. The data have been normalized to the received flux at a microprism angle of 180° to facilitate easier identification of improvements. At this angle, the BEFs degenerate into a slab and become ineffective. The maximum flux occurs at a microprism angle of 100° when the light source is positioned at the center of the panel, resulting in an improvement of over 50% compared to the case where the microprism angle is 180° and the BEFs become ineffective. The efficiency improvement for other source positions also exceeds 50%. The maximum flux for other source positions also occurs in the microprism angle range of 90° to 100° . To provide a more accurate analysis, we conducted simulations for additional cases within the above-mentioned microprism angle range, and the results are presented in Fig. 6(c). The received flux is normalized to the collected data at a 90° microprism angle, which corresponds to the angle of the available BEFs in the market for large-panel LCDs. The average flux across different source positions at the same microprism angle reaches the highest improvement of 5.12% compared to the conventional

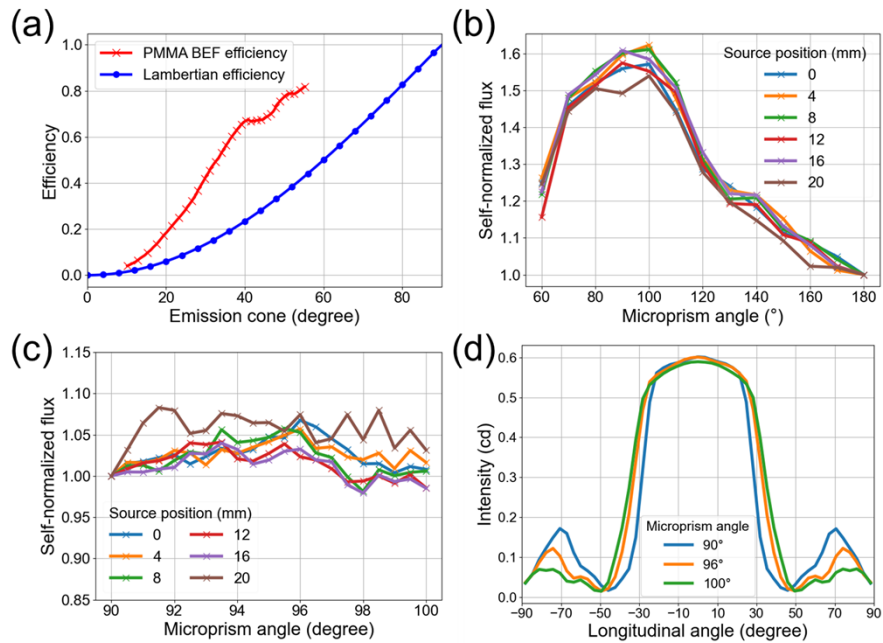


Fig. 6. (a) Efficiency comparison between a Lambertian light source and a BEF-modulated light source. (b) and (c) System flux with BEFs for different microprism angle ranges. (d) Angular distribution after the optimized BEFs in longitudinal direction.

BEFs with a 90° microprism angle when the angle is optimized to 96° . This corresponds to an emission cone of approximately 33° , as shown by the simulation results in Fig. 5(a). The average improvement of the current system with an optimized microprism angle of 96° , compared to systems without BEFs, is 65.2%. The angular distribution of the light source after passing through the BEFs with the optimized microprism angle is illustrated in Fig. 6(d).

3. Conclusion

To enhance the efficiency of the pancake VR system, we first evaluated the impact of the source emission cone on system performance. The emission cone plays a crucial role in determining how light is distributed within the system, affecting the overall brightness and image quality. Additionally, we investigated the performance of BEFs—optical films commonly used for brightness enhancement in traditional LCDs—in modulating the light emission cone. Through simulations with the optimized microprism structure of BEFs, we demonstrated a system efficiency improvement of 65.2% compared to that without BEFs. These simulations indicate that the display emission cone is critical for achieving the desired performance in terms of VR system efficiency.

Disclosures. The authors declare no conflicts of interest.

Data Availability. Data underlying the results presented in this paper are not publicly available at this time but may be obtained from the authors upon reasonable request.

References

1. J. Xiong, E. L. Hsiang, Z. He, *et al.*, “Augmented reality and virtual reality displays: emerging technologies and future perspectives,” *Light:Sci. Appl.* **10**(1), 216 (2021).
2. W. P. Zhang and Z. Wang, “Theory and practice of VR/AR in K-12 science education—a systematic review,” *Sustainability* **13**(22), 12646 (2021).

3. A. A. Rendon, E. B. Lohman, D. Thorpe, *et al.*, "The effect of virtual reality gaming on dynamic balance in older adults," *Age Ageing* **41**(4), 549–552 (2012).
4. S. Choi, K. Jung, and S. D. Noh, "Virtual reality applications in manufacturing industries: past research, present findings, and future directions," *Concurr. Eng.* **23**(1), 40–63 (2015).
5. X. Li, W. Yi, H.-L. Chi, *et al.*, "A critical review of virtual and augmented reality (VR/AR) applications in construction safety," *Autom. Constr.* **86**, 150–162 (2018).
6. J. A. LaRussa and A. T. Gill, "The holographic pancake window TM," *Proc. SPIE* **162**, 120–129 (1978).
7. K. Matsuhashi, T. Kanamoto, and A. Kurokawa, "Thermal model and countermeasures for future smart glasses," *Sensors* **20**(5), 1446 (2020).
8. Z. Yang, Z. Luo, Y. Ding, *et al.*, "Advances and challenges in microdisplays and imaging optics for virtual reality and mixed reality," *Device* **2**(6), 100398 (2024).
9. N. Usukura, K. Minoura, and R. Maruyama, "Novel pancake-based HMD optics to improve light efficiency," *J. Soc. Inf. Disp.* **31**(5), 344–354 (2023).
10. Z. Luo, Y. Ding, Y. Rao, *et al.*, "High-efficiency folded optics for near-eye displays," *J. Soc. Inf. Disp.* **31**(5), 336–343 (2023).
11. Y. Ding, Z. Luo, G. Borjigin, *et al.*, "Breaking the optical efficiency limit of virtual reality with a nonreciprocal polarization rotator," *Opto-Electron. Adv.* **7**(3), 230178 (2024).
12. T. Zhan, E.-L. Hsiang, K. Li, *et al.*, "Enhancing the optical efficiency of near-eye displays with liquid crystal optics," *Crystals* **11**(2), 107 (2021).
13. J. Zou, T. Zhan, E. L. Hsiang, *et al.*, "Doubling the optical efficiency of VR systems with a directional backlight and a diffractive deflection film," *Opt. Express* **29**(13), 20673–20686 (2021).
14. T. Zhan, J. Zou, J. Xiong, *et al.*, "Practical chromatic aberration correction in virtual reality displays enabled by large-size ultra-broadband liquid crystal polymer lenses," *Adv. Opt. Mater.* **8**(2), 1901360 (2020).
15. Z. Luo, Y. Li, J. Semmen, *et al.*, "Achromatic diffractive liquid-crystal optics for virtual reality displays," *Light:Sci. Appl.* **12**(1), 230 (2023).
16. Y. Ding, X. Huang, Y. Ma, *et al.*, "High-efficiency RGB achromatic liquid crystal diffractive optical elements," *Opto-Electron. Adv.* **8**(3), 240181 (2025).
17. E. L. Hsiang, Z. Yang, T. Zhan, *et al.*, "Optimizing the display performance for virtual reality systems," *OSA Continuum* **4**(12), 3052–3067 (2021).
18. E. L. Hsiang, Z. Yang, Q. Yang, *et al.*, "AR/VR light engines: perspectives and challenges," *Adv. Opt. Photon.* **14**(4), 783–861 (2022).
19. R. S. West, H. Konijn, W. Sillevs-Smitt, *et al.*, "High brightness direct LED backlight for LCD-TV," *Dig. Tech. Pap. - Soc. Inf. Disp. Int. Symp.* **34**(1), 1262–1265 (2003).
20. B. Y. Joo and D. H. Shin, "Design guidance of backlight optic for improvement of the brightness in the conventional edge-lit LCD backlight," *Displays* **31**(2), 87–92 (2010).
21. K. P. Capaldo, "Brightness enhancement film, and methods of making and using the same," U.S. Patent 7,251,079 (2007).
22. W. Yuan, L.-H. Li, W.-B. Lee, *et al.*, "Fabrication of microlens array and its application: a review," *Chin. J. Mech. Eng.* **31**(1), 16 (2018).
23. K. Kälántár, "A directional backlight with narrow angular luminance distribution for widening the viewing angle for an LCD with a front-surface light-scattering film," *J. Soc. Inf. Disp.* **20**(3), 133–142 (2012).
24. Y. Gao, Z. Luo, R. Zhu, *et al.*, "A high performance single-domain LCD with wide luminance distribution," *J. Display Technol.* **11**(4), 315–324 (2015).